Long-Range Interactions in the Dimer Interface of Ornithine Decarboxylase Are Important for Enzyme Function†

David P. Myers, Laurie K. Jackson, Vinu G. Ipe, Gavin E. Murphy, and Margaret A. Phillips*

Department of Pharmacology, The University of Texas Southwestern Medical Center at Dallas, 5323 Harry Hines Boulevard, Dallas, Texas 75390-9041

Received July 19, 2001; Revised Manuscript Received August 24, 2001

ABSTRACT: Ornithine decarboxylase (ODC) is a pyridoxal 5′-phosphate dependent enzyme that catalyzes the first committed step in the biosynthesis of polyamines. ODC is a proven drug target for the treatment of African sleeping sickness. The enzyme is an obligate homodimer, and the two identical active sites are formed at the dimer interface. Alanine scanning mutagenesis of dimer interface residues in *Trypanosoma brucei* ODC was undertaken to determine the energetic contribution of these residues to subunit association. Twenty-three mutant enzymes were analyzed by analytical ultracentrifugation, and none of the mutations were found to cause a greater than 1 kcal/mol decrease in dimer stability. These data suggest that the energetics of the interaction may be distributed across the interface. Most significantly, many of the mutations had large effects ($\Delta\Delta G$ k_{cat}/K_m > 2.5 kcal/mol) on the catalytic efficiency of the enzyme. Residues that affected activity included those in or near the substrate binding site but also a number of residues that are distant (15−20 Å) from this site. These data provide evidence that long-range energetic coupling of interface residues to the active site is essential for enzyme function, even though structural changes upon ligand binding to wild-type ODC are limited to local conformational changes in the active site. The ODC dimer interface appears to be optimized for catalytic function and not for dimer stability. Thus, small molecules directed to the ODC interfaces could impact biological function without having to overcome the difficult energetic barrier of dissociating the interacting partners.

Pharmacological manipulation of interactions between proteins could alter many cellular processes but is difficult to achieve. A detailed understanding of the energetics of these interactions is thus needed. Sites of interaction between proteins typically include a large surface area of interacting amino acid residues (*1*), making the task of disrupting the interaction potentially daunting. Systematic mutagenesis of several receptor−ligand protein interfaces has demonstrated that small regions of a protein interface can account for the bulk of the energetic contributions to an interaction (*2*−*6*). These data support the conclusion that the functional epitope driving these interactions is not simply defined by the contacts observed by structural analysis of a protein interface.

Many enzymes form their active sites at the subunit interface and thereby require the association of subunits for activity. Thus interactions that influence the energetics of subunit association may also impact catalytic function, a complexity that is not a component of the receptor−ligand interactions that have been previously studied. Further, this influence may extend beyond amino acid residues that directly participate in the active site structure and involve residues throughout the subunit interface. The energy of binding interactions on proteins can be propagated to remote sites throughout the protein structure (*7*−*9*), and amino acid residues distant from the active site have been shown to impact catalytic efficiency and/or substrate specificity in several enzyme systems (*10*−*14*). However, no systematic analysis of the relationship between the protein interface and catalysis has been undertaken for a multimeric enzyme.

Ornithine decarboxylase (ODC)[1] catalyzes the decarboxylation of L-ornithine to form the diamine putrescine, the first step in the polyamine biosynthetic pathway. The polyamines are ubiquitous cell growth factors, and inhibitors of polyamine biosynthesis have been studied as potential chemotherapeutic agents in a broad range of proliferative diseases, including cancer (*15*) and microbial infections (e.g., African trypanosomiasis *16*). ODC is a pyridoxal 5′-phosphate (PLP) dependent enzyme and an obligate homodimer. The availability of extensive structural and mechanistic information (*17*, *18*) makes ODC an ideal target to study binding interactions at the subunit interface and their relationship to enzyme function. The X-ray structure of *Trypanosoma brucei* ODC reveals two identical active sites that are formed in the dimer interface. Substrate analogues are bound at the interface, making essential contacts with both subunits (Figure 1). The dimer is in rapid equilibrium with the

† This work was supported by grants (to M.A.P.) from the National Institutes of Health (R01 AI34432) and the Welch Foundation (I-1257) and by the National Institutes of Health Medical Scientist Training Program (T32-GM08014 to D.P.M.). M.A.P. is a recipient of a Burroughs Wellcome Fund Scholar Award in Molecular Parasitology.

* To whom correspondence should be addressed. Tel: (214) 648-3637. Fax: (214) 648-9961. E-mail: margaret.phillips@utsouthwestern.edu.

[1] Abbreviations: ODC, ornithine decarboxylase; PLP, pyridoxal 5′-phosphate; DFMO, α-difluoromethylornithine; Orn, L-ornithine; Put, putrescine. *T. brucei* ODC mutant enzymes are designated by single amino acid code, followed by the residue number and by the replacement amino acid.

10.1021/bi0155908 CCC: $20.00
Published on Web 10/10/2001

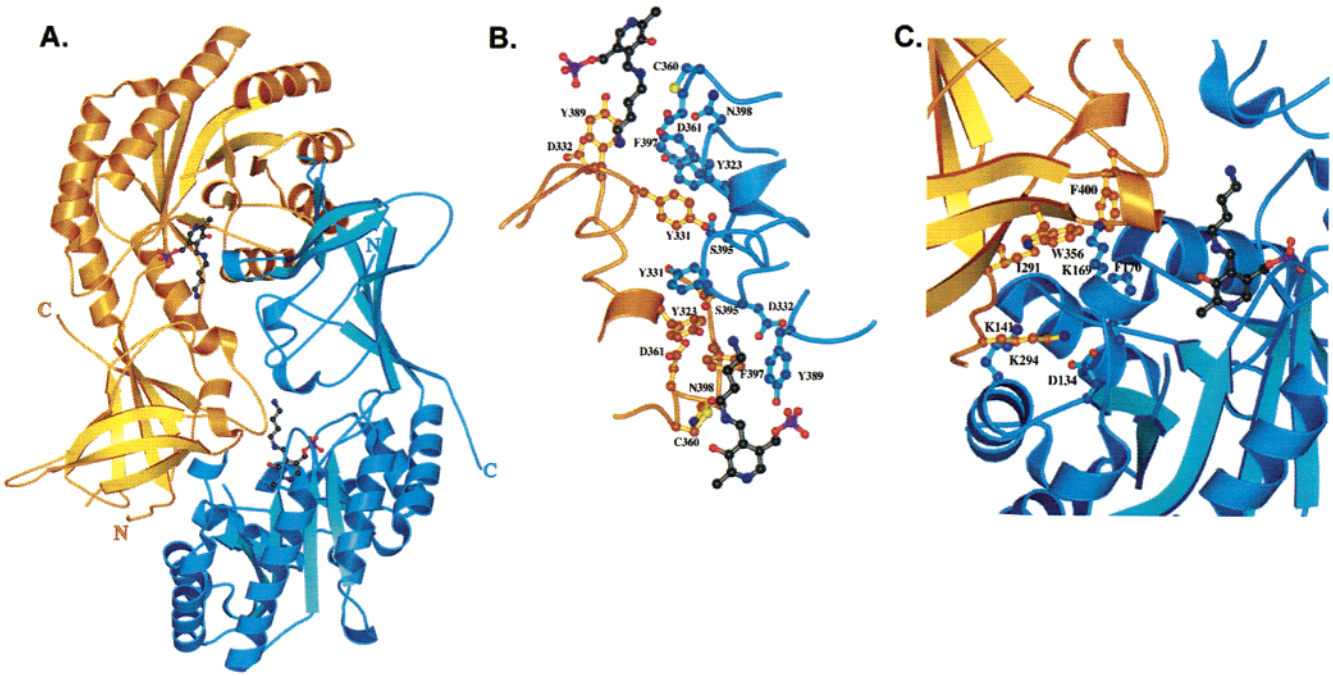

FIGURE 1: X-ray structure of the *T. brucei* ODC active site and dimer interface. (A) Ribbon diagram of the *T. brucei* ODC dimer bound to putrescine (*18*; PDB 1f3t). The monomeric subunits of *T. brucei* ODC are composed of an N-terminal β/α barrel domain and a C-terminal domain that folds into a modified Greek key β-barrel. Two identical active sites are formed in the dimer interface. The N and C termini are marked. (B) The dimer interface region formed between the C-terminal domains of the two subunits. (C) The dimer interface region formed between the N-terminal domain of one subunit and the C-terminal domain of the other. One monomer is displayed in orange, and the other is displayed in blue. The orientation of the subunits is the same in all three panels. Carbon atoms of PLP and of putrescine are displayed in black. Nitrogens are displayed in blue, oxygens are in red, sulfur is in yellow, and phosphate is in pink. The figures were drawn by Molscript and rendered by PovRay (*34*).

monomers, and the functional requirement for contribution of active site residues from both subunits has been demonstrated (*19*).

To evaluate the nature of the interactions that stabilize dimerization of ODC, alanine scanning mutagenesis of *T. brucei* ODC interface residues was undertaken. The wild-type and mutant enzymes were evaluated by sedimentation equilibrium analysis and by steady-state kinetic analysis. None of the mutations caused a significant weakening of the dimer interaction, suggesting that the structural features of the ODC dimer interface that contribute to the energetics of subunit association are distributed throughout the interface. However, mutations of the dimer interface residues caused significant detrimental effects on enzyme activity. These effects were not limited to residues in or near the active site but were distributed throughout the interface.

EXPERIMENTAL PROCEDURES

Materials

Amino acids, amines, buffers, and PLP were purchased from Sigma. Ni^{2+}-agarose was purchased from Qiagen. Centricon concentrators were purchased from Amicon.

Methods

Enzyme Purification and Assay. Site-directed mutagenesis of the ODC DNA was performed using the Quickchange protocol as recommended by the manufacturers (Strategene). All clones were sequenced throughout the entire coding region to verify the mutation. Wild-type and mutant ODCs were expressed from the cloned gene as His-tag fusion proteins in BL21/DE3 cells from the T7 promoter. ODC was purified by Ni^{2+}-agaorose column chromatography and gel filtration as described (*19*, *20*). ODC activity was assayed at 37 °C using a coupled spectrophotometric assay as described (*19*). Enzyme concentrations used for the assay varied depending on the activity of the enzyme. Approximate ranges that were used are as follows: wild-type ODC (5−200 nM), mutants with k_{cat}'s 10-fold below wild type (0.1−0.5 μM), mutants with k_{cat}'s 100-fold below wild type (1−5 μM), and mutants with k_{cat}'s >1000-fold lower than wild type (10−50 μM). Substrate concentrations were collected over a range above and below the K_m for each mutant enzyme. Data were fitted to the Michaelis−Menten equation using Sigma Plot 5.0 to determine the kinetic constants.

Molecular Modeling To Identify Dimer Interface Residues. The X-ray structure of native *T. brucei* ODC (PDB 1QU4) and of the DFMO-bound enzyme (PDB 2tod) were used to analyze the nature of the amino acid residues at the dimer interface. Interface residues were identified by calculating the change in solvent-accessible surface area between the dimer and monomer using the program NACCESS (*36*).

Analytical Ultracentrifugation. Analytical ultracentrifugation was performed in a Beckman XLI centrifuge. ODC samples were analyzed in 100 mM Hepes, pH 7.5, 100 mM NaCl, 0.5 mM 2-mercaptoethanol, and 20 μM PLP at 20 °C. A minimum of three ODC concentrations (ranging from 3.5 to 14 μM) were used for each analysis. For equilibrium sedimentation analysis ODC was loaded into a six-sector equilibrium centerpiece, and the protein was equilibrated for data collection at three rotor speeds (11000, 13 000, and 15 000 rpm). Once equilibrium had been reached (typically

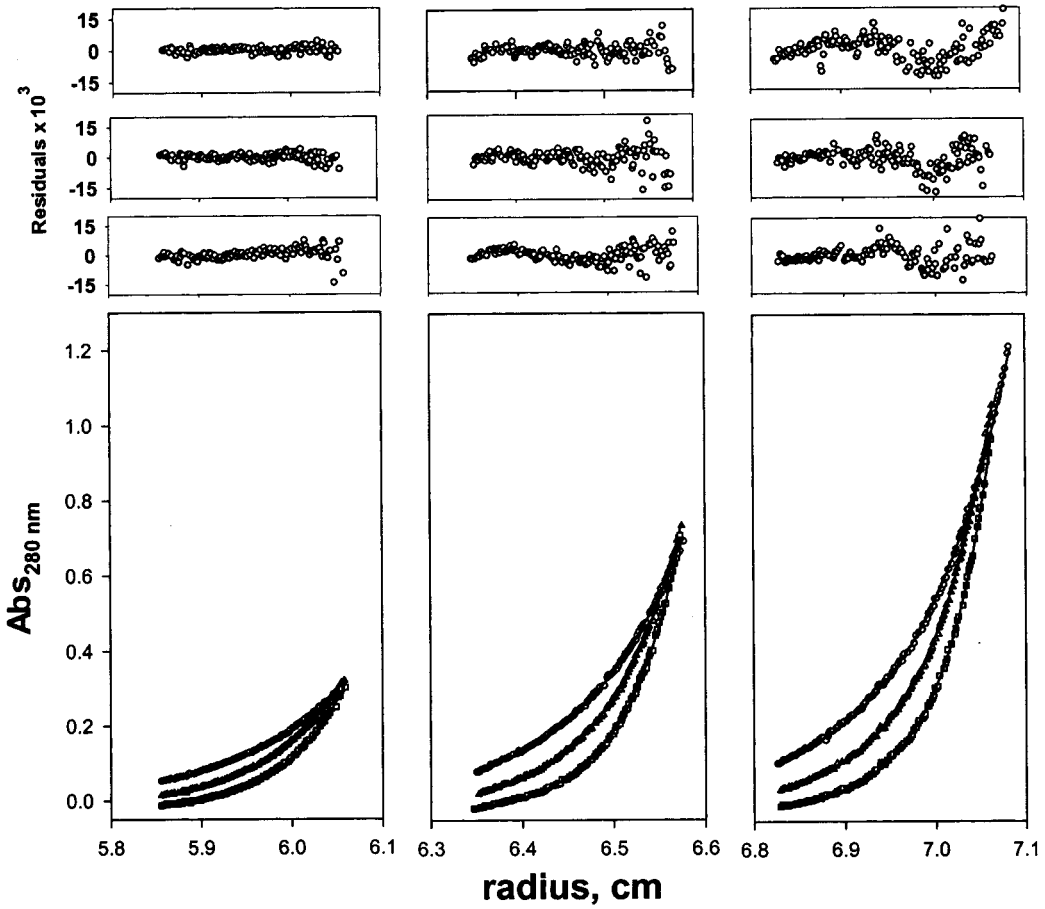

FIGURE 2: Representative sedimentation equilibrium data set collected for wild-type ODC. Sedimentation data (open symbols) were collected in a Beckman XLI analytical ultracentrifuge. The data in the figure include nine data sets used in the global analysis for a representative fit to determine the K_d for dimer dissociation. The monomer molecular mass was fixed at 49 050 Da during the fit, and the baseline values were allowed to float. The panels (from left to right) represent three ODC concentrations (4.8, 9.6, and 14.4 μM). For each ODC concentration, three speeds [from left to right 11 000 (circles), 13 000 (triangles), and 15 000 (squares) rpm]) were collected. The solid line represents the weighted global fit to a monomer/dimer equilibrium with K_d = 341 nM and 95% confidence limits of 250−460 nM. The residuals to the fit are shown in the upper panel in absorbance units. The dimerization constant (K_d = 406 ± 92 nM) for wild-type ODC was calculated by averaging the model-derived K_d's from n = 6 independent experiments where the error is the standard deviation of the mean.

24−36 h), absorption data were collected through quartz windows at 280 nm, using a radial step size of 0.001 cm, and recorded as the average of 15 measurements at each radial position. To determine the baseline values in the cell, at the end of the data collection time the rotor speed was increased to 42 000 rpm for 8 h, and the absorbance of the depleted meniscus was measured (over-speed data).

Equilibrium data were analyzed using the Beckman XL-A/XL-I Data Analysis Software Version 4.0. A minimum of nine data sets were included in the global nonlinear least-squares analysis using a monomer−dimer equilibrium model (eq 1) to determine the dimer association constant (K_{Aa}). The

$$c_r = c_0^{Mon} e^{(\omega^2/2RT)M(1-\bar{v}\rho)(r^2-r_0^2)} + K_{Aa}(c_0^{Mon})^2 e^{(\omega^2/2RT)2M(1-\rho)(r^2-r_0^2)} \quad (1)$$

monomer mass (M = 49 050) was fixed during the analysis, and the baseline values were allowed to float. Parameters for eq 1 are as follows: c_r is the concentration in absorbance units at the radial position r, c_0 is the concentration of the monomer at a reference radius r_0, ω is the angular velocity in radians per second, R is the gas constant 8.314 × 10^7 erg·K^{-1}·mol^{-1}, T is the temperature in kelvin, M is the gram molecular weight, $\bar{v}$ is the partial specific volume, ρ is the density of the solvent, and K_{Aa} is the association constant in absorption units. $\bar{v}$ (0.735 mL·g^{-1}) and ρ (1.00 g·mL^{-1}) were fixed during the fit to values determined using the program SEDNTERP (*21*). K_{Aa} is converted to the dissociation constant (K_d) in concentration units of monomer by the equation:

$$K_d = \frac{2}{K_{Aa} b \epsilon} \quad (2)$$

where b is the path length (1.2 cm) and ϵ (41 690 M^{-1}·cm^{-1}) is the experimentally determined molar extinction coefficient (*19*). For the W356A mutant ϵ was instead 36 000 M^{-1}·cm^{-1}.

RESULTS

Analysis of Wild-Type ODC Dimerization by Analytical Ultracentrifugation. Wild-type *T. brucei* ODC was analyzed by equilibrium sedimentation centrifugation. For each experiment data were collected for three rotor speeds and three ODC concentrations as described in Experimental Procedures. The data were best fit by the model describing a self-associating system for a monomer/dimer equilibrium. A representative data set is displayed in Figure 2. The dimerization constant (K_d = 406 ± 92 nM) for the wild-type

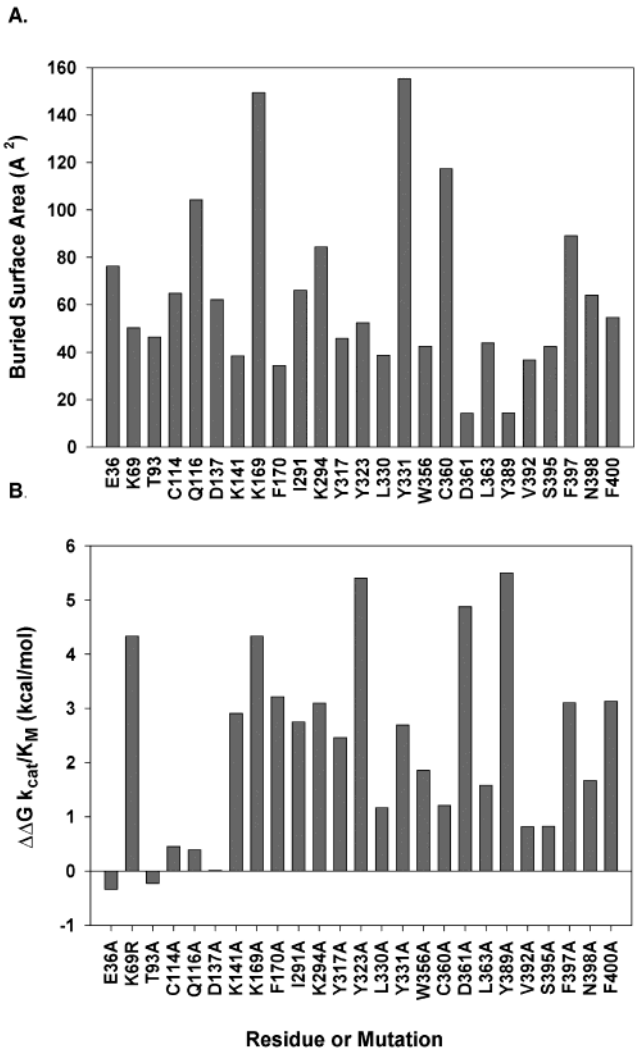

FIGURE 3: Analysis of ODC dimer interface residues. (A) Total buried surface area (Å^2) for interface residues upon formation of dimeric *T. brucei* ODC. Buried surface area was determined by calculating the change in solvent-accessible surface area between the dimer and monomer using the program NACCESS. The data calculated for the native *T. brucei* ODC structure (PDB 1QU4) is displayed. With the exception of the two active site residues, Y389 and D361, alanine mutants of all of these residues were evaluated by analytical ultracentrifugation. (B) The energetic differences in catalytic efficiency of the interface mutants compared to the wild-type enzyme are plotted, where $\Delta\Delta G_{k_{cat}/K_m} = -RT \ln[(k_{cat}/K_m)^{mutant}/(k_{cat}/K_m)^{wt}]$. ODC activity was assayed at 37 °C using a coupled spectrophotometric assay as described (*19*). Values for D361A, K69R, and C360 were previously reported (*18*, *22*, *23*).

enzyme was determined on the basis of the analysis of multiple ($n = 6$) data sets of this type. The full range of ODC concentrations (3.5−14. 4 μM) was explored within these data sets.

Analysis of Dimer Interface Mutations by Analytical Ultracentrifugation. The X-ray structure of native *T. brucei* ODC was used to identify residues in the dimer interface. The change in solvent-accessible surface area between the dimer and monomer was calculated using the program NACCESS. A total of 2775 Å^2 of solvent-accessible surface area is buried in the interface upon dimerization (*17*); 87% of the surface area is contributed by amino acid side chains (Figure 3A). The ODC dimer interface is formed by interactions between the C-terminal domains of the two subunits and between the N-terminal and C-terminal domains of opposite subunits (Figure 1; *17*). A row of aromatic residues (F397, Y323, and Y331) that pass through the 2-fold axis and is positioned between the two active sites, makes up the bulk of the contact between the two C-terminal domains. The interface between the N-terminal and C-terminal domains of the two subunits contains the active site and is partially composed of hydrophilic interactions between amino acid side chains and/or backbone carbonyls (e.g., D134/K294, D364/K169, and I291/K141).

Amino acid residues identified to contribute >35 Å^2 of surface area to the interface in both the native and DFMO-bound structures by this analysis were mutated to Ala (Figure 3A) to determine the contribution of these side chains to the energetics of the subunit association. The dimer dissociation constants (K_d) for each of the mutant ODCs were determined by analytical ultracentrifugation by collecting a standard data set of three concentrations and three speeds for each mutant as described in Experimental Procedures. The K169A mutation could not be evaluated because the protein failed to come to equilibrium despite multiple attempts, a finding that may be a reflection of reduced stability for this mutant enzyme. None of the mutations that could be evaluated increased the K_d for dimerization by more than 3-fold compared to the wild-type value. For several of the mutant enzymes (E36A, K69A, C114A, W356A, V392A, and S395A) the K_d's determined for the monomer−dimer equilibrium were approximately 10-fold lower than measured for the wild-type enzyme. For such monomer−dimer equilibria the theoretical concentration of monomer present in the analysis is near the limit of detection [the lower limit of K_d that can be measured is 10 nM (*22*)], and the accuracy of the method is reduced.

Kinetic Analysis of the Dimer Interface Mutations. The active site of ODC is formed at the dimer interface, suggesting that residues in the dimer interface may also be important for the catalytic function of the enzyme. To address this question, steady-state kinetic analysis of the wild-type and mutant enzymes was undertaken to determine the Michaelis−Menten parameters for the decarboxylation of L-ornithine. Mutation of 18 of the tested interface residues decreased k_{cat}/K_m by at least 1 kcal/mol (Table 1, Figure 4). Predictably, the residues where mutation had the largest effects ($\Delta\Delta G_{k_{cat}/K_m}$ > 4 kcal/mol) are located in the active site and participate in either direct contacts with substrate/analogues or contact mediated through a water molecule [e.g., K69, Y323, D361, Y389, and F397 (Figure 1B)]. The roles of several of these active site residues (K69, C360, and D361) have previously been well characterized (*18*, *23*, *24*). However, mutation of a number of residues that are distant from the active site also had large detrimental effects (2−3 kcal/mol) on enzyme activity (Table 1 and Figure 4). These long-range effects occurred predominately in the interface region formed by contacts between the N- and C-terminal domain (Figure 1C, residues K141, I291, K294, Y317, and W356), and they effect both k_{cat} (decreases by 2−40-fold) and K_m (increases 3−20-fold). The most striking examples of these long-range effects are for residues K141, I291, and K294, all of which are 15−20 Å from the nearest active site (Figure 1C and Table 1).

The specific activity (V_{max}/E_T) of wild-type ODC is constant between enzyme concentrations of 5−200 nM (data not shown), suggesting that the K_d for dimer dissociation is

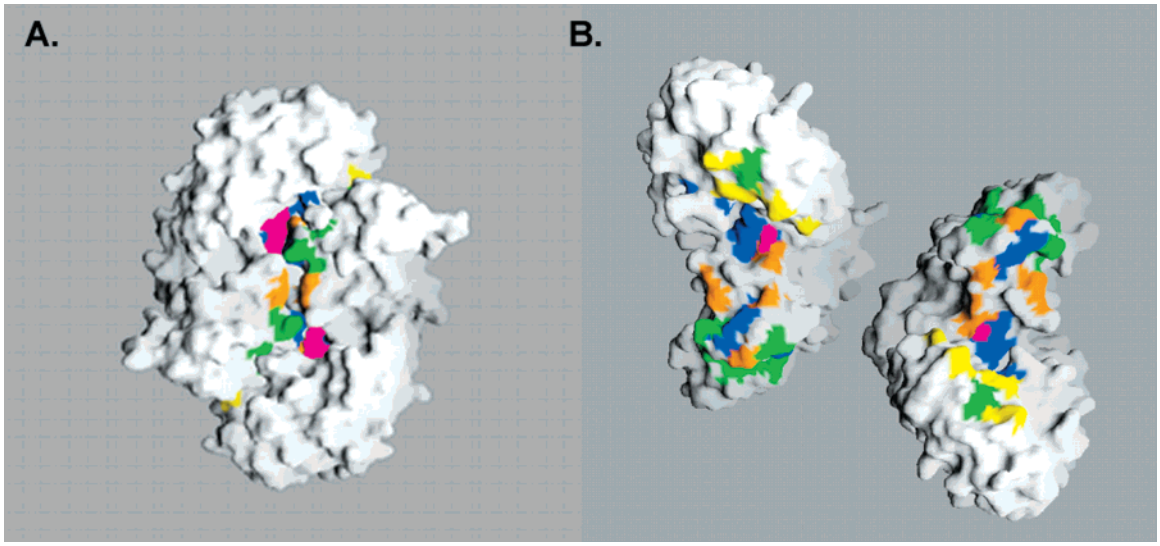

FIGURE 4: Energetic map of the kinetic effects of the *T. brucei* ODC dimer interface mutations. (A) The color-coded energetic changes ($\Delta\Delta G$) due to alanine substitution of interface residues are plotted for k_{cat}/K_m. (B) The monomers have been separated by 40 Å, and each has been rotated 90° toward the observer. The values for $\Delta\Delta G$ were calculated as described in Figure 3. Images were generated using the program GRASP (*35*). $\Delta\Delta G$ values are displayed as follows: yellow, −0.2 to 0.5 kcal/mol; orange, 0.6−1.5 kcal/mol; green, 1.6−3.0 kcal/mol; blue, >3.0 kcal/mol. Putrescine is displayed in pink as a marker for the active site.

Table 1: Kinetic Parameters for ODC Interface Mutants

enzyme	k_{cat}[a] (s^{-1})	K_m[a] (mM)	k_{cat}/K_m (s^{-1} mM^{-1})	$\Delta\Delta G$ k_{cat}/K_m (kcal·mol^{-1})	distance (Å) to active site[d]
wt ODC	9.4 ± 0.1	0.49 ± 0.04	19		
E36A	5.5 ± 0.1	0.17 ± 0.02	33	−0.34	20−25
K69R[b]	0.0031 ± 0.0003	0.18 ± 0.40	0.017	4.3	3.3−5
T93A	5.7 ± 0.0	0.21 ± 0.016	28	−0.24	15−20
C114A	4.5 ± 0.1	0.49 ± 0.03	9.0	0.46	5−10
Q116A	6.3 ± 0.2	0.62 ± 0.09	10	0.39	10−15
D137A	9.7 ± 0.3	0.50 ± 0.04	20	−0.01	15−20
K141A	0.26 ± 0.0	1.5 ± 0.1	0.17	2.9	15−20
K169A	0.10 ± 0.00	5.8 ± 1.5	0.017	4.3	5−10
F170A	5.0 ± 1.1	47 ± 14	0.11	3.2	5−10
I291A	1.9 ± 0.2	8.3 ± 1.3	0.23	2.7	10−15
K294A	0.71 ± 0.05	5.6 ± 1.7	0.13	3.1	10−15
Y317A	0.92 ± 0.01	2.6 ± 0.09	0.35	2.5	10−15
Y323A	0.042 ± 0.002	16 ± 2	0.003	5.4	3.3−5
L330A	2.7 ± 0.1	0.93 ± 0.04	2.9	1.2	5−10
Y331A	6.0 ± 0.3	25 ± 3	0.24	2.7	3.3−5
W356A	1.6 ± 0.1	1.7 ± 0.4	1.0	1.8	10−15
C360A[b]	0.27 ± 0.0	0.10 ± 0.01	2.7	1.2	3.3−5
D361A[b]	3.1 ± 1.0	450 ± 170	0.007	4.9	3.3−5
L363A	3.4 ± 0.2	2.3 ± 0.8	1.5	1.6	5−10
Y389A[c]	<0.003	nd	<0.003	>5.5	<3.3
V392A	0.97 ± 0.08	0.19 ± 0.03	5.1	0.81	5−10
S395A	0.59 ± 0.04	0.12 ± 0.03	5.0	0.82	10−15
F397A	0.028 ± 0.001	0.31 ± 0.04	0.90	3.1	3.3−5
N398A	0.27 ± 0.01	0.210 ± 0.025	1.3	1.7	5−10
F400A	0.014 ± 0.000	0.12 ± 0.011	0.12	3.1	10−15

[a] Errors are the standard deviation of the mean ($n = 3$). [b] Values for D361A, K69R, and C360 were previously reported (*18*, *23*, *24*). [c] Measured at 10 mM L-ornithine. [d] Distances were measured between the nearest atom on PLP or putrescine and the nearest atom of the amino acid residue. Data are reported for six different shells where this distance is within the shell: <3.3 Å, 3.3−5 Å, 5−10 Å, 10−15 Å, 15−20 Å, and 20−25 Å.

less than 5 nM in the conditions of the assay, which is minimally 80-fold lower than observed in the analytical ultracentrifuge. However, there are several notable differences between the assay conditions and those used to analyze dimer formation by analytical ultracentrifuge. First, the presence of substrate may affect dimer association. Second, the enzyme activity is measured at 37 °C while the centrifugation studies were performed at 20 °C and at higher ionic strength. For most of the mutant enzymes the specific activity was also constant over the range of enzyme concentrations tested. However, because many of the mutant enzymes are significantly less active than the wild-type enzyme, the concentration of enzyme used for the activity assay (see Experimental Procedures) was much higher and thus does not allow for a comparison of dimer stability under the conditions of the assay. For I291A ODC the specific activity does not reach maximal levels for enzyme concentrations below 50−100 nM, suggesting that, in contrast to what was observed by centrifugation, the K_d for the dimer under the conditions of the assay is weaker than for the wild-type enzyme.

DISCUSSION

ODC is an obligate homodimer with the substrate binding sites formed at the dimer interface (Figure 1). X-ray structure analysis facilitates identification of the residues that make contacts at the dimer interface, but the energetic contribution of the individual residues to subunit association can only be addressed by functional analysis. Alanine scanning mutagenesis of the *T. brucei* ODC dimer interface suggests that no single amino acid in the interface contributes more than 1 kcal/mol of stabilizing energy to the interaction. These data suggest that the subunit association is driven by many small energetic contributions distributed throughout the interface. These results are in contrast to the interaction "hot spots" observed in some previously studied systems. Analyses of several protein interfaces by mutagenesis [e.g., the growth hormone−receptor interaction (*2*, *3*), antibody interactions with antigen (*4*, *5*), and the barnase−barnstar interaction (*6*)] indicated that small regions of a protein interface can account for the bulk of the energetic contributions to an interaction.

The finding that no significant energetic consequences are observed upon mutation of dimer interface residues in ODC may be an indication of structural plasticity in the interface. Structural analysis of the antigen−antibody system and of the barnase−barnstar interaction suggests that mutations can

be accommodated by the incorporation of water molecules at the site of the mutation (*4*, *25*). Additionally, the detrimental effects of mutating a key residue in the growth hormone receptor could be complemented by a mutation in the hormone that allowed for repacking of the interface (*8*). The ODC interface may accommodate the mutations by similar mechanisms. Structural plasticity may be particularly important for the function of an interface that is associated with a catalytic cycle and may be necessary for accommodation of the substrate into the interface in a catalytically competent state.

In contrast to the limited disruptive effects caused by the mutations of the dimer interface residues, a number of the mutations (E36A, K69A, C114A, W356A, V392A, and S395A) appear to strengthen the dimer. The kinetic data suggest that the dimer may also be strengthened in the presence of substrate. The structural basis for these effects is not clear; however, these mutations may cause local conformational changes that affect the electrostatic or dipole interactions between the subunits either directly or indirectly. In support, an analysis of interfacial hydrogen bonds and salt bridges in protein−protein interfaces suggested that residues involved in these interactions might not be oriented in their global minimum conformations (*26*). Thus mutation of residues in the interface could cause repacking of the interface that leads to optimization of these interactions.

The most significant effects of mutating residues in the dimer interface were on enzyme activity. Many of the largest effects on activity of interface mutations can be ascribed to proximity to the active site, an obvious reflection of the fact that many of these residues play a role in the binding of substrate or the chemistry of the reaction (*17*, *18*). Likewise, the mutation of second-sphere residues (e.g., K169, F170, and N398) could disrupt active site architecture and impede catalysis. Similar effects have been described in other systems and typically involve the disruption of a hydrogen bond network (*12*, *14*). Indeed, K169 forms a salt bridge across the dimer interface with the backbone carbonyls of D361 and D364, while F170 also makes contacts with this region. These interactions are likely to play a key role in stabilizing the loop that contains both C360 and D361, two key active site residues.

However, interface mutations with large catalytic consequences were not limited to the first- and second-sphere residues of the active site. Mutation of a number of peripheral interface residues (e.g., K141, I291, K294, Y317, and W356) that are 15−20 Å away from the active site significantly reduced the catalytic efficiency of the enzyme. Interestingly, many of these residues are contained in the same region of the interface (e.g., the backbone carbonyl of I291 and the side chain of K141 form an H-bond across the interface). The effects of these mutations were observed on both k_{cat} and K_m. Both parameters potentially reflect multiple steps in the reaction pathway, including Schiff base formation and/or the chemical steps of the reaction. These data provide evidence for long-range energetic coupling of the interface residues to the active site. Taken together with the dimerization data, these data suggest that the subunit interactions in ODC are optimized for catalytic function and not for high-affinity subunit association. The data leave open the possibility that the energetic contribution of the interface residues to dimer strength may be distributed differently in the presence of substrate or product. In support, kinetic analysis of the I291A mutant enzyme suggested that the dimer was weaker than for wild-type ODC, while the sedimentation data collected in the absence of substrate did not.

The structural basis for the coupling of dimer interface residues and the active site is likely to be subtle. X-ray structural analysis of *T. brucei* ODC in the absence and presence of putrescine demonstrates that the conformational changes that are observed upon putrescine binding are limited to local rotational changes in two catalytic residues in the active site. C360 rotates toward the bound ligand, and as the Schiff base between K69 and PLP is exchanged for the Schiff base to substrate, K69 rotates away from the cofactor to form new interactions (*18*). However, unlike what has been observed upon binding of ligands to some enzymes [e.g., dihydrofolate reductase (*27*), thymidylate synthase (*28*, *29*), aspartate amino transferase (*30*)], no domain rotations or global repositioning of loops or structural elements have been observed upon binding of putrescine or DFMO to ODC (*17*, *18*). Long-range effects on catalysis of mutating surface loop residues in dihydrofolate reductase are related to a network of interactions that form between these distant loops and a mobile active site loop structure that has conformational flexibility (*14*). In contrast for ODC, the structural data suggest that the propagation of small structural or electronic changes are likely to be sufficient to account for the coupling of catalytic efficiency to the interface energetics. Orbital overlap is thought to be a major driving force of catalysis, and small structural changes in bonding overlap have been demonstrated to be sufficient to cause large catalytic deficits in enzyme-catalyzed reactions (*31*). Likewise, dimer interface mutations that disrupt ODC activity may cause suboptimal orientation of the π-orbitals of the cofactor−substrate complex, a critical factor in catalysis by PLP-dependent enzymes (*32*).

T. brucei ODC is a drug target for the treatment of African trypanosomiasis (*16*). Inhibitors that could either dissociate the dimer or bind in the dimer interface and disrupt activity would have advantages over traditional active site directed inhibitors. For example, protein interfaces of multimeric enzymes do not tend to be highly conserved (*33*), suggesting that greater selectivity could be obtained by targeting the subunit interface. Inhibitors that dissociate the ODC dimer might be found, but the lack of discrete regions of the interface that drive the energetics of the interaction may limit this approach. However, the observation that mutations in the interface at sites distant from the active site disrupt enzyme activity suggests that an inhibitor would not have to dissociate the dimer to be effective. Rather, a small molecule could bind and disrupt activity by a mechanism of induced allostery. Ultimately, this latter approach may prove to be more generally useful, since it may be easier to find ligands that bind in the dimer interface and disrupt activity than to identify molecules that can effectively compete and disrupt a protein−protein interaction.

ACKNOWLEDGMENT

We thank Jennifer Ford for technical assistance in the data collection and John Philo, Joe Albanesi, Dirk Binns, Rama Ranganathan, and Jeff Baldwin for helpful discussions.

REFERENCES

1. Conte, L. L., Chothia, C., and Janin, J. (1999) *J. Mol. Biol. 285*, 2177−2198.
2. Clackson, T., and Wells, J. A. (1995) *Science 267*, 383−386.
3. Clackson, T., Ultsch, M. H., Wells, J. A., and de Vos, A. M. (1998) *J. Mol. Biol. 277*, 1111−1128.
4. Dall'Acqua, W., et al. (1998) *Biochemistry 37*, 7981−7991.
5. Jin, L., and Wells, J. A. (1994) *Protein Sci. 3*, 2351−2357.
6. Schreiber, G., and Fersht, A. R. (1995) *J. Mol. Biol. 248*, 478−486.
7. Freire, E. (1999) *Proc. Natl. Acad. Sci. U.S.A. 96*, 10118−10122.
8. Atwell, S., Ultsch, M., De Vos, A. M., and Wells, J. A. (1997) *Science 278*, 1125−1128.
9. Lockless, S. W., and Ranganathan, R. (2000) *Science 286*, 295−299.
10. Oue, S., Okamoto, A., Yano, T., and Kagamiyama, H. (1999) *J. Biol. Chem. 274*, 2344−2349.
11. Hedstrom, L., Sylagi, L., and Rutter, W. J. (1992) *Science 255*, 1249−1253.
12. Jeffrey, C. J., Gloss, L. M., Petsko, G. A., and Ringe, D. (2000) *Protein Eng. 13*, 105−112.
13. LiCata, V. J., and Ackers, G. K. (1995) *Biochemistry 34*, 3133−3138.
14. Miller, G. P., and Benkovic, S. J. (1998) *Chem. Biol. 5*, R105−R113.
15. Marton, L. J., and Pegg, A. E. (1995) *Annu. Rev. Pharmacol. Toxicol. 35*, 55−91.
16. Wang, C. C. (1995) *Annu. Rev. Pharmacol. Toxicol. 35*, 93−127.
17. Grishin, N. V., Osterman, A. L., Brooks, H. B., Phillips, M. A., and Goldsmith, E. J. (1999) *Biochemistry 38*, 15174−15184.
18. Jackson, L. K., Brooks, H. B., Osterman, A. L., Goldsmith, E. J., and Phillips, M. A. (2000) *Biochemistry 39*, 11247−11257.
19. Osterman, A. L., Grishin, N. V., Kinch, L. N., and Phillips, M. A. (1994) *Biochemistry 33*, 13662−13667.
20. Brooks, H. B., and Phillips, M. A. (1997) *Biochemistry 36*, 15147−15155.
21. Laue, T. M., Shah, B., Ridgeway, T. M., and Pelletier, S. L. (1992) in *Analytical Ultracentrifugation in Biochemistry and Polymer Science* (Harding, S., Rowe, A., and Horton, J., Eds.) pp 90−125, Royal Society of Chemistry, Cambridge.
22. Hensley, P. (1996) *Structure 4*, 367−373.
23. Osterman, A., Kinch, L. N., Grishin, N. V., and Phillips, M. A. (1995) *J. Biol. Chem. 270*, 11797−11802.
24. Osterman, A. L., Brooks, H. B., Jackson, L., Abbott, J. J., and Phillips, M. A. (1999) *Biochemistry 38*, 11814−11826.
25. Vaughan, C. K., Buckle, A. M., and Fersht, A. R. (1999) *J. Mol. Biol. 286*, 1487−1506.
26. Xu, D., Tsai, C. J., and Nussinov, R. (1997) *Protein Eng. 10*, 999−1012.
27. Sawaya, M. R., and Kraut, J. (1997) *Biochemistry 36*, 586−603.
28. Kamb, A., Finer-Moore, J. S., and Stroud, R. M. (1992) *Biochemistry 31*, 12876−12884.
29. Matthews, D. A., Villafranca, J. E., Janson, C. A., Smitth, W. W., Welsh, K., and Freer, S. (1990) *J. Mol. Biol. 214*, 937−948.
30. Kirsch, J. F., Eichele, G., Ford, G. C., Vincent, M. G., and Jansonius, J. N. (1984) *J. Mol. Biol. 174*, 497−525.
31. Mesecar, A. D., Stoddard, B. L., and Koshland, D. E. (1997) *Science 277*, 202−206.
32. Dunathan, H. C. (1966) *Proc. Natl. Acad. Sci. U.S.A. 55*, 712−716.
33. Grishin, N. V., and Phillips, M. A. (1994) *Protein Sci. 3*, 2455−2458.
34. Esnousf, B. M. (1997) *J. Mol. Graphics 15*, 133−138.
35. Nicholls, A., Bharadwaj, R., and Honig, B. (1993) *Biophys. J. 64*, A166−A166.
36. Hubbard, S. J., and Thornton, J. M. (1993) NACCESS, Computer Program, Department of Biochemistry and Molecular Biology, University College London, at http://sjh.bi.umist.ac.uk/naccess.html.

BI0155908